



Inverse effects of APOC2 and ANGPTL4 on the conformational dynamics of lid-anchoring structures in lipoprotein lipase

Anni Kumari^{ab} , Anne Louise Grønnemose^{abc} , Kristian K. Kristensen^{ab} , Anne-Marie L. Winther^{ab} , Stephen G. Young^{d,e,1} , Thomas J. D. Jørgensen^c , and Michael Ploug^{a,b,1}

Contributed by Stephen G. Young; received January 3, 2023; accepted March 28, 2023; reviewed by Arun Radhakrishnan and Rudolf Zechner

The lipolytic processing of triglyceride-rich lipoproteins (TRLs) by lipoprotein lipase (LPL) is crucial for the delivery of dietary lipids to the heart, skeletal muscle, and adipose tissue. The processing of TRLs by LPL is regulated in a tissue-specific manner by a complex interplay between activators and inhibitors. Angiopoietin-like protein 4 (ANGPTL4) inhibits LPL by reducing its thermal stability and catalyzing the irreversible unfolding of LPL's α/β -hydrolase domain. We previously mapped the ANGPTL4 binding site on LPL and defined the downstream unfolding events resulting in LPL inactivation. The binding of LPL to glycosylphosphatidylinositol-anchored high-density lipoprotein-binding protein 1 protects against LPL unfolding. The binding site on LPL for an activating cofactor, apolipoprotein C2 (APOC2), and the mechanisms by which APOC2 activates LPL have been unclear and controversial. Using hydrogen–deuterium exchange/mass spectrometry, we now show that APOC2's C-terminal α -helix binds to regions of LPL surrounding the catalytic pocket. Remarkably, APOC2's binding site on LPL overlaps with that for ANGPTL4, but their effects on LPL conformation are distinct. In contrast to ANGPTL4, APOC2 increases the thermal stability of LPL and protects it from unfolding. Also, the regions of LPL that anchor the lid are stabilized by APOC2 but destabilized by ANGPTL4, providing a plausible explanation for why APOC2 is an activator of LPL, while ANGPTL4 is an inhibitor. Our studies provide fresh insights into the molecular mechanisms by which APOC2 binds and stabilizes LPL—and properties that we suspect are relevant to the conformational gating of LPL's active site.

APOC2 | HDX-MS | intravascular lipolysis | GPIHBP1 | ANGPTL4

Genetic and epidemiologic studies have uncovered a causal relationship between plasma levels of triglyceride-rich lipoproteins (TRL) and the risk of coronary heart disease [CHD] (1–3). Multivariable Mendelian Randomization studies have suggested that this relationship is independent of low-density lipoprotein cholesterol levels (4, 5). Lipoprotein lipase (LPL) is crucial for the intravascular hydrolysis of triglycerides in TRLs. The pivotal role of LPL in plasma triglyceride metabolism is evident from the fact that genetic deficiencies in LPL and other genes supporting LPL function (*APOC2*, *APOA5*, *LMF1*, *GPIHBP1*) cause severe hypertriglyceridemia (chylomicronemia), along with a predisposition to acute pancreatitis (6). In contrast, loss-of-function variants in genes encoding proteins that inhibit LPL or otherwise interfere with TRL processing (e.g., *ANGPTL3*, *ANGPTL4*, *ANGPTL8*, *APOC3*) reduce plasma triglyceride levels and reduce CHD risk (7–10). The latter observations have inspired new strategies to reduce plasma triglyceride levels and CHD risk (5, 11).

While some of the key proteins for intravascular triglyceride metabolism were discovered decades ago—LPL in 1955 (12) and its cofactor apolipoprotein C2 (APOC2) in 1970 (13)—we have only recently gleaned insights into mechanisms for regulating and compartmentalizing LPL activity (14–16). Progress includes: i) the crystal structure of LPL (17); ii) the discovery that LPL is active as a monomer (18, 19); iii) the recognition that LPL is metastable at body temperature, resulting in rapid loss of activity due to irreversible unfolding of LPL's α/β -hydrolase domain (20–22); and iv) the discovery that a physiologic inhibitor, angiopoietin-like protein 4 (ANGPTL4), inactivates LPL by binding to LPL's α/β -hydrolase domain and triggering conformational changes that lead to irreversible unfolding and loss of catalytic activity (14, 21, 23–25). Whether the inhibition of LPL activity in oxidative tissues (e.g., heart, skeletal muscle) by the ANGPTL3-ANGPTL8 complex (26–28) also triggers accelerated LPL unfolding is currently unknown.

Studies on LPL's endothelial cell binding protein, glycosylphosphatidylinositol-anchored high-density lipoprotein-binding protein 1 (GPIHBP1), provided additional insights into the regulation and compartmentalization of LPL activity in capillaries (14, 15, 29). GPIHBP1 shuttles newly secreted LPL from the subendothelial spaces to its site of action

Significance

The processing of triglyceride-rich lipoproteins (TRLs) by lipoprotein lipase (LPL) is the central event in plasma lipid metabolism. Inefficient TRL processing causes hypertriglyceridemia and increases the risk of coronary heart disease. A plasma protein, apolipoprotein C2 (APOC2), activates LPL, but the understanding of APOC2-LPL interactions has been incomplete. Here we mapped, by hydrogen–deuterium exchange/mass spectrometry, the binding interface between APOC2 and LPL. We also showed that APOC2 augments LPL's thermal stability and stabilizes the sequences that anchor LPL's lid (which controls substrate entry into the catalytic pocket). Our studies illuminated APOC2-LPL molecular interactions and could ultimately be useful for developing strategies to augment LPL activity and increase the efficiency of TRL processing.

Author contributions: A.K. and M.P. designed research; A.K., A.L.G., K.K.K., and A.-M.L.W. performed research; A.K. contributed new reagents/analytic tools; A.K., A.L.G., K.K.K., A.-M.L.W., S.G.Y., T.J.D.J., and M.P. analyzed data; and A.K., S.G.Y., T.J.D.J., and M.P. wrote the paper.

Reviewers: A.R., The University of Texas Southwestern Medical Center; and R.Z., Karl-Franzens-Universität Graz.

Competing interest statement: A.R. is one of the reviewers. For the past 3 y, A.R. and S.G.Y. have participated in a consortium grant sponsored by the Leducq Foundation. Our projects differ but both of our projects are related to cholesterol metabolism.

Copyright © 2023 the Author(s). Published by PNAS. This article is distributed under Creative Commons Attribution-NonCommercial-NoDerivatives License 4.0 (CC BY-NC-ND).

¹To whom correspondence may be addressed. Email: sgyoung@mednet.ucla.edu or m-ploug@finsenlab.dk.

This article contains supporting information online at <https://www.pnas.org/lookup/suppl/doi:10.1073/pnas.2221888120/-/DCSupplemental>.

Published April 24, 2023.

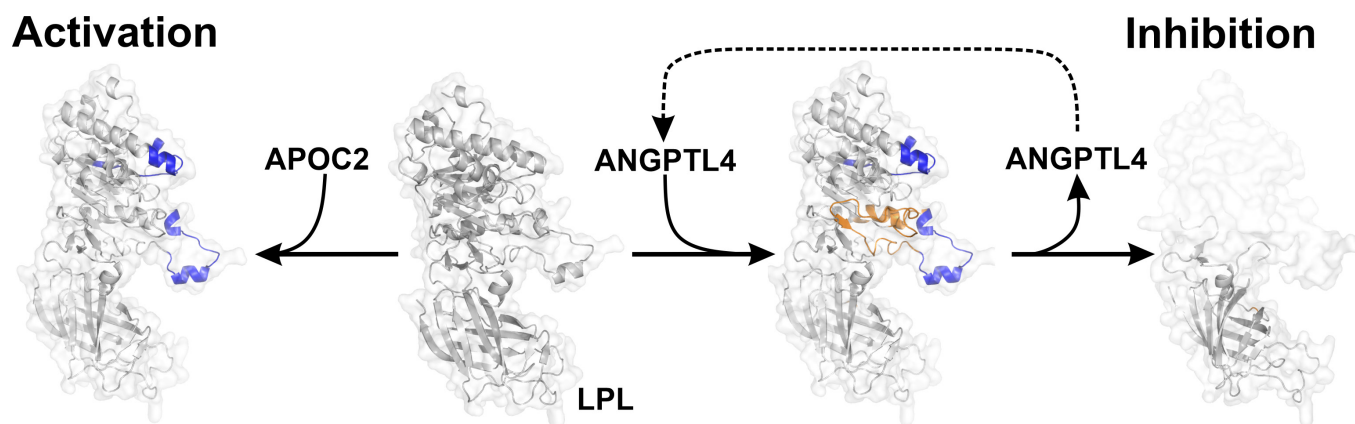


Fig. 1. Regulation of LPL activity by APOC2 and ANGPTL4. APOC2 and ANGPTL4 share overlapping binding sites on LPL (highlighted blue) but have inverse impacts on LPL activity. ANGPTL4 inhibits LPL activity by catalyzing the irreversible unfolding of LPL's α/β -hydrolase domain (transparent surface). APOC2 binds to the same regions of LPL but results in LPL activation. Our HDX-MS studies provide the first mechanistic insights into this conundrum: ANGPTL4 and APOC2 have different effects on LPL metastability and the conformational dynamics of structures surrounding the catalytic triad and structures that anchor LPL's lid.

in the capillary lumen (30), where LPL is important for TRL margination (31). Biallelic loss-of-function variants in *GPIHBP1* (32–34)—as well as GPIHBP1 autoantibodies—cause chylomicronemia (35, 36). GPIHBP1 is an atypical member of the Ly6/uPAR (LU) protein domain family inasmuch it contains a 42-residue highly acidic and intrinsically disordered N-terminal extension upstream from its canonical LU domain (37). Biophysical studies with purified proteins and physiological studies in genetically modified mice revealed that the intrinsically disordered acidic domain is important for LPL function (14, 29, 38). The acidic domain increases the association rate constant (k_{on}) for LPL binding by >2,500-fold (38), increases the thermostability of LPL by >20 °C (21, 22); mitigates Angiopoietin-like protein 4 (ANGPTL4)-catalyzed LPL unfolding (21, 23, 39), and establishes an electrostatic “charge relay mechanism” that allows LPL to detach from heparan sulfate proteoglycans in the interstitial spaces (38) and move to higher affinity binding sites on capillary endothelial cells (29).

We now have a vastly improved understanding of molecular mechanisms governing LPL, GPIHBP1, and ANGPTL4 interactions, but we have only limited insights into how APOC2 binds and activates LPL (Fig. 1). APOC2 is a 79-amino acid plasma apolipoprotein that is required for LPL-mediated TRL processing—evident from the fact that biallelic loss-of-function *APOC2* mutations cause severe chylomicronemia (40). NMR studies and molecular dynamics simulations revealed that a 26-residue amphipathic α -helix I (residues 13 to 39) associates with lipids, while a C-terminal α -helix III (residues 58 to 79) associates with lipids only at the nanosecond time scale (41–43). Site-directed mutagenesis studies revealed that Tyr⁶³, Ile⁶⁶, Asp⁶⁹, and Gln⁷⁰ (all located in α -helix III) are important for LPL activation (44), but the location of APOC2's binding site(s) on LPL has been uncertain and controversial (45–47). In the current study, we mapped APOC2's binding site on LPL by hydrogen–deuterium exchange/mass spectrometry (HDX-MS), and we assessed the impact of APOC2 on the conformational stability of LPL's α/β -hydrolase domain. We found that APOC2 binds to regions surrounding the catalytic pocket in LPL, including the lid. Remarkably, APOC2 and ANGPTL4 have overlapping binding sites on LPL, but they have dramatically different effects on LPL conformation. APOC2 stabilizes the architecture of the catalytic pocket and the sequences that anchor LPL's lid, whereas ANGPTL4 results in progressive unfolding of those

regions and leads to irreversible inactivation of the enzyme. We also assess the impact of APOC2 on LPL in the presence of two physiologically relevant binding partners—GPIHBP1 and ANGPTL4.

Results

LPL Binding Stabilizes α -Helix III in APOC2. To understand the biophysical basis for LPL•APOC2 interactions, we expressed and purified four recombinant APOC2 proteins: APOC2^{wt}, APOC2^{Y63E}, APOC2^{Q70E}, and APOC2^{L72P}. To facilitate purification, all proteins contained an N-terminal 6 \times His-tag; this modification has no effect on APOC2's ability to activate LPL (44). The ability of APOC2^{Q70E} to activate LPL was negligible (Fig. 2A), consistent with earlier findings (44). Using long-chain triacylglycerol emulsions as a substrate, 0.4 μ M APOC2^{Q70E} failed to activate LPL hydrolysis (Fig. 2A), whereas 0.04 μ M APOC2^{wt} was sufficient to trigger half-maximal LPL activation (Fig. 2B). Under these conditions, APOC2^{wt} activated GPIHBP1-bound LPL as efficiently as free LPL (Fig. 2B). In all subsequent experiments, APOC2^{Q70E} was used as negative control.

In the absence of lipids, APOC2 is intrinsically disordered and prone to amyloid fibrillization (48, 49), but a 50-fold molar excess of dodecyl phosphocholine (DPC) mitigates amyloid formation (48). Using circular dichroism (CD) and dynamic light scattering (DLS) studies (Fig. 2C–E), we determined the minimal amounts of 1,2-dimyristoyl-*sn*-glycero-3-phosphocholine (DMPC) required to induce maximal helicity in APOC2 (i.e., APOC2's native conformation). A molar ratio of 1:50 of APOC2^{wt} to DMPC was both necessary and sufficient to induce maximal APOC2 helicity (Fig. 2C). This molar ratio converted 49-nm DMPC vesicles into 7-nm micelles, as judged by DLS (Fig. 2E). Under these conditions, the CD spectra for APOC2^{wt} and APOC2^{Q70E} were identical (Fig. 2D), indicating that the inability of APOC2^{Q70E} to activate LPL was not due to an inability to form amphipathic α -helices in the presence of DMPC. Importantly, the APOC2–DMPC formulation was compatible with HDX-MS analyses; online pepsin cleavage of the APOC2–DMPC yielded 29 unique APOC2 peptides with a sequence coverage of 86.2% (SI Appendix, Fig. S1).

To localize regions in APOC2 that form α -helices in the presence of DMPC, we incubated 3 μ M APOC2^{wt} or APOC2^{Q70E} (with and without DMPC) in deuterated solvent (20 mM Tris, 150 μ M DMPC, and 150 mM NaCl in 70% deuterium oxide, pH_{read} 8.0) at 25 °C and then measured time-dependent

[†]In this article, amino acid numbering starts with the first residue of the mature protein.

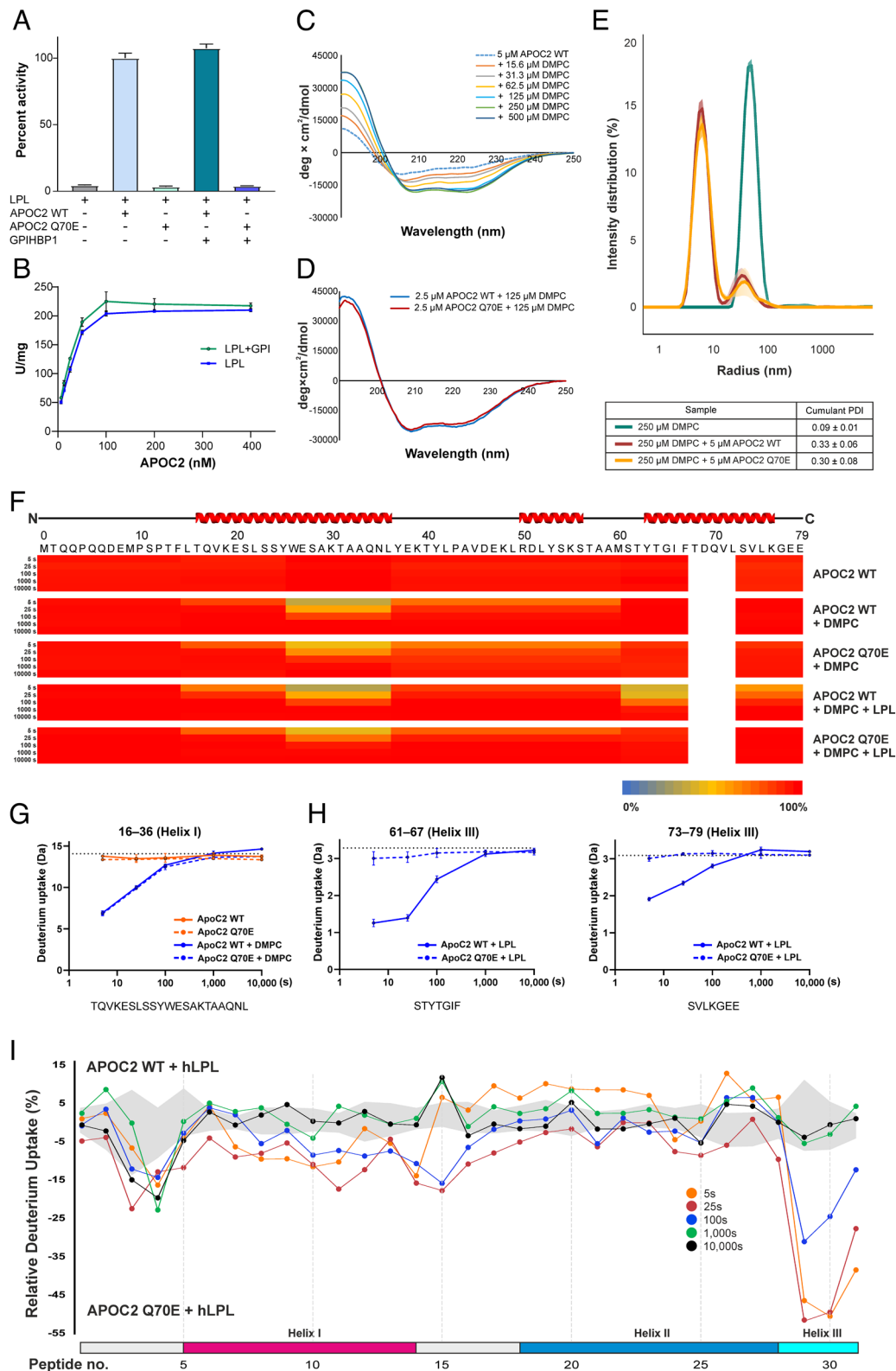


Fig. 2. APOC2 is intrinsically disordered, but DMPC stabilizes α -helices I and II and LPL stabilizes α -helix III. (A) Hydrolysis of long-chain triacylglycerol emulsions by 6 nM LPL or 6 nM LPL+GPIHBP1 complexes in the presence of 0.4 μ M APOC2^{WT} or 0.4 μ M APOC2^{Q70E}. (B) Concentration-dependent stimulation in the lipase activity of 6 nM LPL and 6 nM LPL+GPIHBP1 complexes by APOC2^{WT}. (C) Helicity of APOC2^{WT} in the presence of increasing amounts of DMPC, as assessed by local minima at 208 nm and 222 nm by circular dichroism. (D) Comparison of APOC2^{WT} or APOC2^{Q70E} in the presence of DMPC by circular dichroism. (E) Disappearance of 49-nm DMPC vesicles following the addition of APOC2^{WT} or APOC2^{Q70E}, as measured by dynamic light scattering. (F) Heat maps for deuterium uptake in 3 μ M APOC2^{WT} or 3 μ M APOC2^{Q70E} by continuous labeling in the presence or absence of 150 μ M DMPC; upper three panels show DMPC-mediated stabilization of α -helices I and II in APOC2. Lower two panels show the specific stabilization of α -helix III in 3 μ M APOC2^{WT} in 150 μ M DMPC by 4.5 μ M LPL^{S132A/R297A}, as assessed by continuous labeling. Protection of α -helix III was absent with APOC2^{Q70E}. (G) Deuterium uptake in α -helix I (peptide 26 to 36), revealing identical impacts of DMPC on APOC2^{WT} and APOC2^{Q70E}. (H) LPL reduces deuterium uptake in α -helix III (peptides 61 to 67 and 73 to 79) of APOC2^{WT} but not APOC2^{Q70E}. (I) Butterfly plot showing differential deuterium uptake in APOC2^{WT} (compared to APOC2^{Q70E}) in the presence of LPL. Uptake values were calculated relative to 100% deuterium controls. The shaded gray area corresponds to the largest SD in the dataset for each peptide (n = 3).

deuterium incorporation by HDX-MS (Fig. 2 *F* and *G*). In the absence of DMPC, all backbone amide groups in APOC2 were maximally labeled after the shortest exchange time (5 s), consistent with the intrinsically disordered state of APOC2 in the absence of lipids. The presence of DMPC provided strong protection against deuterium uptake in APOC2 peptides from α -helix I (residues 16 to 38) and moderate protection in peptides covering α -helix II (residues 50 to 56) but no protection against deuterium uptake in α -helix III (residues 63 to 76). These findings are consistent with previous data from NMR relaxation and nuclear Overhauser effect studies with ^{13}C - and ^{15}N -labeled APOC2 in the presence of sodium dodecyl sulfate or DPC (42, 43). We observed only very minor differences in deuterium uptake in APOC2^{wt} and APOC2^{Q70E} in the presence of DMPC, indicating that both proteins have comparable interactions with DMPC (*SI Appendix, Figs. S2 and S3*).

Having established an optimal formulation of APOC2 in DMPC, we went on to use HDX-MS to define the binding site for LPL on APOC2. We incubated 3 μM APOC2^{wt} or APOC2^{Q70E} in 150 μM DMPC with 4.5 μM human LPL^{S132A/R297A} in a deuterated solvent. In these experiments, we used an inactive LPL with a catalytic triad mutation (Ser¹³²→Ala) to eliminate confounding effects of myristic acid [which is released from DMPC when LPL^{wt} is incubated with APOC2^{wt} (*SI Appendix, Fig. S4*)]. The inactive LPL contained a second mutation (Arg²⁹⁷→Ala) to eliminate a furin cleavage site. Neither LPL thermostability nor LPL•GPIHBP1 binding kinetics was affected by these mutations (22). Our HDX-MS experiments revealed that LPL protects against deuterium uptake in APOC2 α -helix III (residues 61 to 79; peptides Ser⁶¹–Phe⁶⁷ and Ser⁷³–Glu⁷⁹) (Fig. 2 *F, H, and I* and *SI Appendix, Fig. S5*). APOC2 α -helix III contains all of the residues that had been identified by alanine-scanning mutagenesis to be required for APOC2's cofactor activity (i.e., Tyr⁶³, Ile⁶⁶, Asp⁶⁹, Gln⁷⁰) (44). Our HDX-MS findings refined the interpretation of earlier mutagenesis studies; they revealed that the failure of APOC2^{Q70E} to activate LPL is due to the fact that APOC2^{Q70E} lacks the ability to interact with LPL.

Defining the Binding Sites on LPL for APOC2 by Continuous Labeling HDX-MS. To identify the binding site(s) for APOC2 on LPL, we incubated 3 μM LPL^{S132A/R297A} with 4.5 μM APOC2^{wt} or APOC2^{Q70E} for 5, 25, 100, 1,000 and 10,000 s at 25 °C in deuterated solvent (20 mM Tris, 225 μM DMPC, and 150 mM NaCl in 70% deuterium oxide, pH_{read} 8.0). We used LPL^{S132A/R297A} to avoid DMPC hydrolysis. Hydrogen–deuterium exchange was quenched by acidification at low temperature. Online pepsin digestion followed by mass spectrometry recovered 82 peptic peptides covering 92.9% of human LPL (*SI Appendix, Fig. S6*). We optimized the HDX-MS protocol to assess deuterium uptake in LPL as a function of APOC2^{wt} binding (using APOC2^{Q70E} mutant as a negative control). The deuterium uptake in LPL in the setting of APOC2^{wt} or APOC2^{Q70E} was probed 5, 25, 100, 1,000, and 10,000 s in deuterated solvent and visualized by heat maps, butterfly plots, and deuterium-uptake plots (Fig. 3 and *SI Appendix, Fig. S7*).

Consistent with earlier studies with bovine LPL (14, 19, 20), purified human LPL is metastable and undergoes unfolding after prolonged incubations (1,000 or 10,000 s) at 25 °C. LPL unfolding in the presence of deuterated solvent is evident by the accumulation of bimodal isotope envelopes in peptic peptides from the α/β -hydrolase domain [amino acids 61 to 72 ($\alpha 2$ - $\beta 3$), 100 to 111 ($\alpha 3$), 129 to 163 ($\beta 4$ - $\alpha 4$ - $\beta 5$), and 178 to 184 ($\beta 6$)]. These regions are highlighted by dark gray bars in the heat maps shown in Fig. 3*A* and are visualized on the LPL crystal structure shown

in *SI Appendix, Fig. S8A*. Of note, spontaneous unfolding of LPL was mitigated by APOC2^{wt} but not APOC2^{Q70E} (*SI Appendix, Fig. S9*). At first glance, APOC2-mediated stabilization of LPL appeared similar to the stabilizing effects of GPIHBP1 (14, 19, 21, 38, 50); however, as we discuss later, the effects of APOC2 and GPIHBP1 on LPL conformation are distinct.

Given the propensity of LPL to unfold during prolonged incubations at 25 °C, we focused on short incubation times (5, 25, 100 s) to map APOC2's binding interface on LPL. At those time points, LPL unfolding in the presence of APOC2^{wt} or APOC2^{Q70E} was negligible (Fig. 3). APOC2^{wt} retarded EX2-mediated deuterium uptake (defined by unimodal isotope shifts[†]) in four regions of LPL. All four regions are exposed on one surface of LPL's α/β -hydrolase domain as visualized on the LPL structure (*SI Appendix, Fig. S8B*) and marked with cyan bars in Fig. 3*A* and *B*. The deuterium uptake profile allowed us to infer that APOC2^{wt} binds to and/or stabilizes LPL at residues 50 to 60 (connecting $\beta 2$ and $\alpha 2$), residues 87 to 99 (connecting $\beta 3$ and $\alpha 3$), residues 185 to 217 ($\beta 7$ and connection to the lid), and residues 218 to 236 (lid) (*SI Appendix, Figs. S7 and S8B*). APOC2 binding to the lid at 5 to 25 s was unequivocal and highly significant, but it was also highly dynamic; deuterium uptake was nearly maximal after 100 s (Fig. 3*B* and *C*). Unexpectedly, three of the four sites in LPL that are protected by APOC2 were shown previously to be binding sites for ANGPTL4 (21), a physiologic inhibitor of LPL that catalyzes the irreversible unfolding of LPL's α/β -hydrolase domain (14, 23). This observation posed a conundrum: How could an LPL inhibitor (ANGPTL4) and an LPL activator (APOC2) bind to overlapping sites yet have opposite effects on LPL stability and activity? We do not yet have a complete answer to this question, but our current HDX-MS experiments provided an important insight. Our HDX-MS study revealed that APOC2 and ANGPTL4 have opposite effects on the dynamics of LPL sequences that anchor the lid to the α/β -hydrolase domain. APOC2^{wt} reduced deuterium uptake in LPL segments 185 to 217 ($\beta 7$ and connecting loops) and 237 to 247 ($\alpha 5$) by retarding EX2 deuterium exchange kinetics (Fig. 3 and *SI Appendix, Fig. S10*). In contrast, ANGPTL4 increased EX2 exchange kinetics in the same regions (21). The ability of ANGPTL4 to destabilize residues 185 to 217 ($\beta 7$ and connecting loops) is noteworthy. In studies of spontaneous LPL unfolding (*SI Appendix, Figs. S7–S10*), we observed distinct onsets for deuterium uptake in different regions of LPL's hydrolase domain. From these studies, it was clear that global unfolding in regions 61 to 72 ($\alpha 2$ - $\beta 3$), 100 to 111 ($\alpha 3$), 129 to 163 ($\beta 4$ - $\alpha 4$ - $\beta 5$), 178 to 184 ($\beta 6$), and 287 to 314 ($\beta 10$ - $\beta 1$) occurs *after* the increased dynamics in 185 to 217 ($\beta 7$ with connecting loops)—as visualized in *SI Appendix, Fig. S8A*. Thus, increased dynamics in $\beta 7$ and connecting loops, which occur with ANGPTL4 but not APOC2, could enhance LPL's metastability by lowering the threshold for global unfolding of the α/β -hydrolase domain. APOC2 binding also reduced deuterium uptake in the other lid-anchoring site [237 to 247 ($\alpha 5$)], although that effect was evident only at later time points due to a relatively higher inherent stability of that region (Fig. 3*C*).

APOC2 Activation of GPIHBP1-bound LPL. In a physiologic context, APOC2 on circulating TRLs likely encounters LPL complexed to GPIHBP1 along capillaries (29–31). To create an in vitro surrogate for this scenario, we performed a continuous labeling experiment with 2.2 μM LPL^{S132A/R297A} and 3 μM

[†]EX1-type kinetics occur when transient local or global unfolding of LPL exposes a number of backbone amide hydrogens to the solvent and the exchange-competent amides are exposed for a sufficient time to allow them to undergo simultaneous isotopic exchange (i.e., correlated exchange) before refolding occurs. In EX2-type kinetics, the exchange-competent open conformation of LPL has a short lifetime compared to the time required for isotopic exchange. Therefore, LPL needs to “visit” the open conformation numerous times for deuterium exchange to occur.

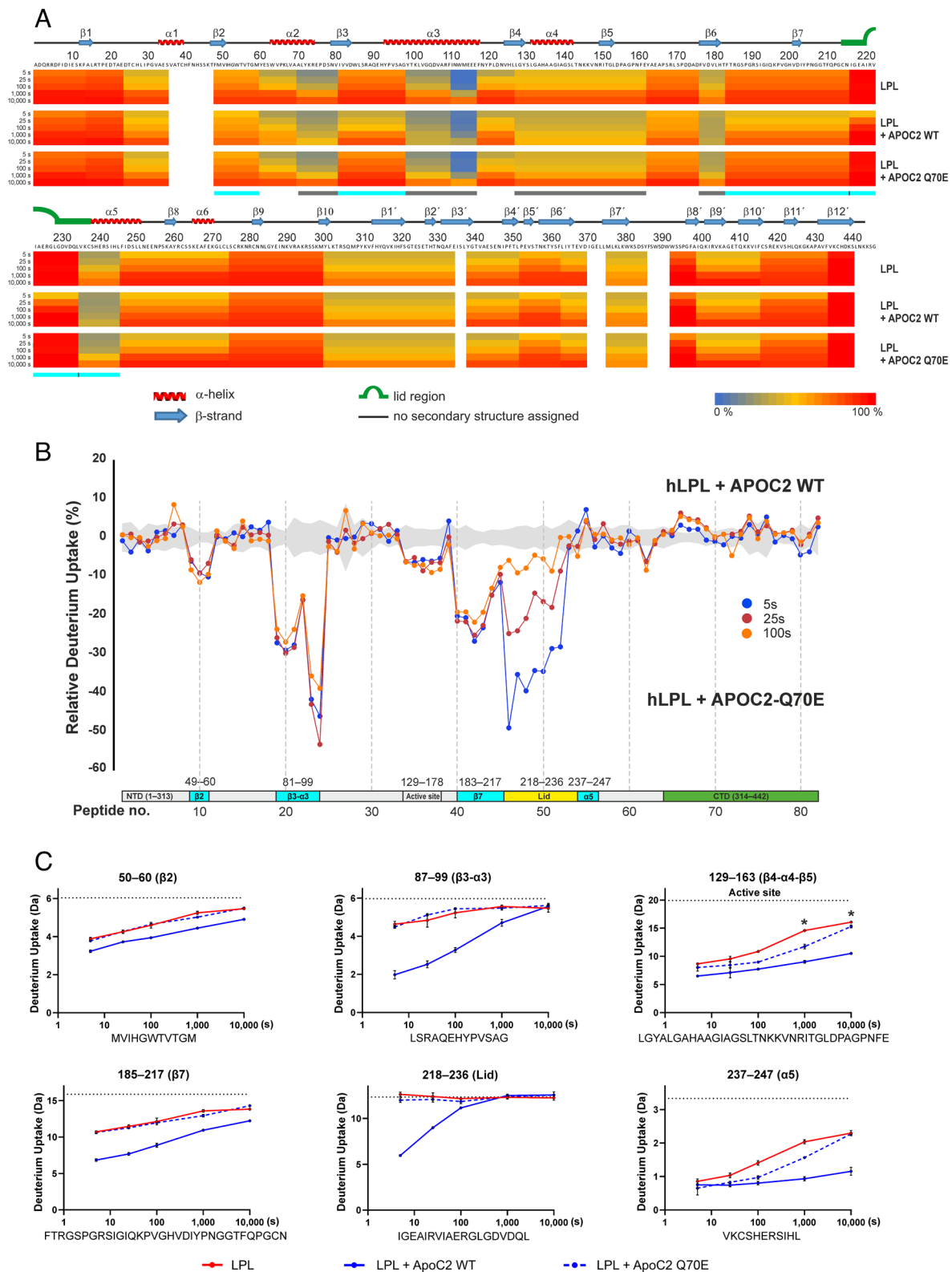


Fig. 3. Localizing the APOC2 binding site on LPL. (A) Heat maps portraying progressive deuterium incorporation into LPL peptides relative to a fully deuterated control. The data reports on the time-dependent deuterium uptake during continuous labeling of $3 \mu\text{M}$ LPL^{S132A/R297A} in the presence or absence of $4.5 \mu\text{M}$ APOC2^{WT} or APOC2^{Q70E} in $225 \mu\text{M}$ DMPC for 5, 25, 100, 1,000, or 10,000 s at 25°C ($n = 3$). Secondary structures, shown above the primary sequence, are from the LPL crystal structure (17). Binding sites, as defined by reduced deuterium uptake via EX2 kinetics (unimodal isotope envelopes) at shorter incubation times, are highlighted by cyan bars. Stabilizing effects slowing deuterium uptake by EX1 kinetics (bimodal isotope envelopes), which were particularly evident at longer incubation times, are highlighted by gray bars. (B) Butterfly plots showing the differential deuterium uptake in 83 peptic peptides derived from LPL^{S132A/R297A} that was incubated in deuterium oxide at 25°C in the presence of APOC2^{WT} or APOC2^{Q70E} for 5, 25, or 100 s (continuous labeling). Peptides covering selected structural regions in LPL are identified by the lower bar, while regions displaying altered EX1 or EX2 deuterium uptake kinetics are highlighted by the thin gray and cyan bars, respectively. (C) Time-dependent deuterium uptake in selected peptic peptides from LPL^{S132A/R297A} incubated in deuterium oxide alone (red) or in the presence of either APOC2^{WT} (blue) or APOC2^{Q70E} (green). Levels representing 100% deuterium uptake are shown by the dotted lines. Asterisk marks the emergence of bimodal isotope envelopes with EX1 kinetics.

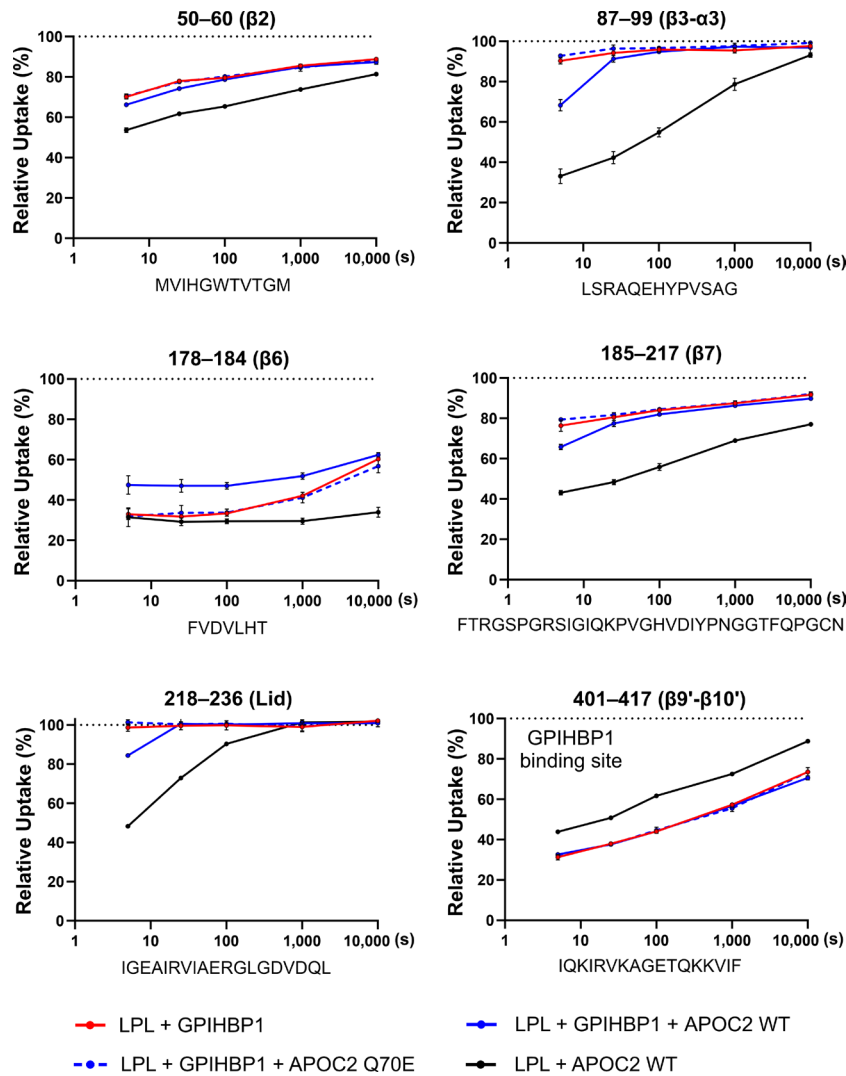


Fig. 4. APOC2 binding to LPL•GPIHBP1 complexes. Time-dependent deuterium uptake in peptic LPL peptides from 2.2 μM LPL^{S132A/R297A} with 3 μM GPIHBP1 incubated in deuterium oxide alone (red) or in the presence of 3 μM APOC2^{WT} (blue) or APOC2^{Q70E} (broken blue line). Data on LPL^{S132A/R297A} in the presence of APOC2^{WT} (black) was imported from Fig. 3. To facilitate comparison between experiments, levels of deuterium uptake are calculated relative to 100% deuteration controls. The absolute deuterium uptake values and heatmap are shown in *SI Appendix, Figs. S11 and S12*.

GPIHBP1 in the presence of 3 μM APOC2^{WT} or APOC2^{Q70E} in 150 μM DMPC for 5, 25, 100, 1,000, or 10,000 s at 25 °C. This GPIHBP1 concentration greatly exceeds the K_D for GPIHBP1•LPL interactions (0.3 nM) (38); hence, we expected that the LPL would be saturated with GPIHBP1 throughout the experiment. Consistent with that expectation, regions of LPL that interface with GPIHBP1 (e.g., residues 401 to 417) exhibited reduced deuterium uptake throughout the labeling period (Fig. 4). Although APOC2 binding changed deuterium uptake in LPL whether or not the LPL was bound to GPIHBP1 (Fig. 4), we observed differences when LPL was complexed to GPIHBP1. First, the ability of APOC2^{WT} to protect against deuterium uptake in LPL was weaker when GPIHBP1 was present (Fig. 4 and *SI Appendix, Figs. S11 and S12*). Second, LPL residues 178 to 184 (β_6) exhibited increased deuterium uptake when both APOC2^{WT} and GPIHBP1 were present, whereas neither APOC2^{WT} alone nor GPIHBP1 alone had this effect (Fig. 4). The biologic significance of the latter observation is unclear, but it probably helps to explain the fact that APOC2^{WT} was more effective in reducing deuterium uptake in free LPL than in GPIHBP1-bound LPL. In any case, APOC2 stimulated hydrolysis of long-chain

triacylglycerol emulsions to a similar degree whether or not LPL was complexed to GPIHBP1 (Fig. 2A).

APOC2 Binding Increases LPL Thermostability. Prompted by the observation that spontaneous unfolding of LPL at 25 °C was delayed by APOC2^{WT} (*SI Appendix, Fig. S9*), we used pulse-labeling HDX-MS to assess the impact of APOC2 on the thermal stability of LPL. We incubated 6.7 μM LPL^{S132A/R297A} with 10 μM APOC2^{WT} or APOC2^{Q70E} in 500 μM DMPC for 4 min at 10 °C, 20 °C, 30 °C, or 40 °C before a 10-s pulse labeling in deuterated solvent at 25 °C, followed by quenching and HDX-MS analyses. For comparison, we analyzed 6.7 μM LPL^{S132A/R297A} in the presence of 10 μM APOC2^{Q70E} and 10 μM GPIHBP1. In the presence of APOC2^{Q70E}, the emergence of bimodal isotope envelopes in peptide 132 to 163 (harboring LPL's active site Ser¹³²) was robust at 30 °C, and the transition to the high-mass populations was complete at 40 °C (Fig. 5A). In contrast, when LPL was incubated with APOC2^{WT}, we did not observe an increase in bimodality in peptide 132 to 163 at 40 °C (Fig. 5A). This experiment revealed a stabilizing effect of APOC2 binding on the thermal unfolding of LPL. In this experiment, APOC2^{WT}

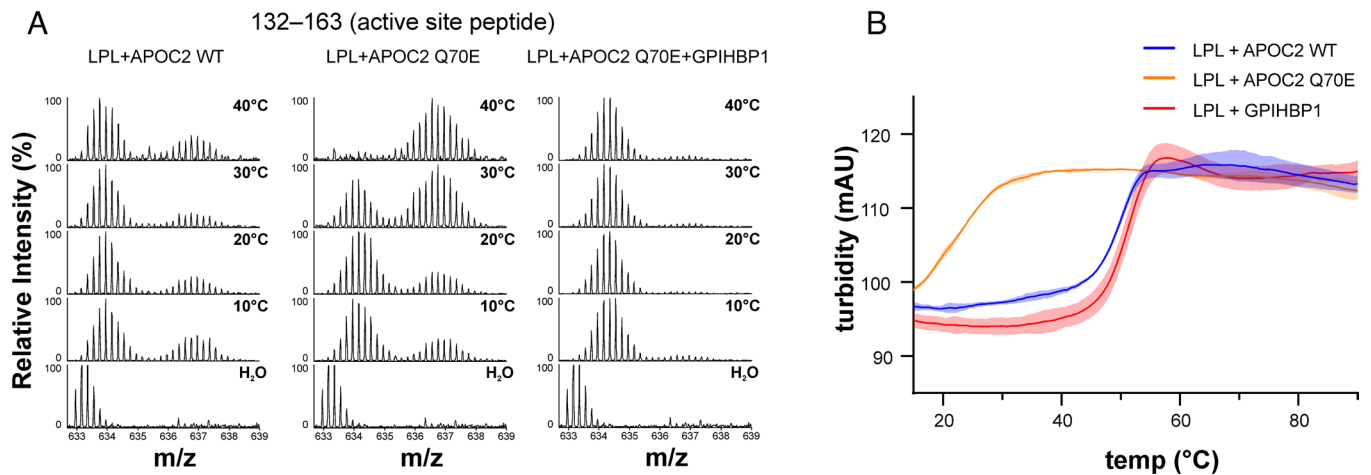


Fig. 5. Impact of APOC2 on thermal unfolding of LPL. (A) Pulse deuterium labeling for 10 s at 25 °C of 6.67 μM LPL^{S132A/R297A} that had been pre-incubated for 240 s with 10 μM APOC2^{WT}, APOC2^{Q70E}, or GPIHBP1 at 10 °C, 20 °C, 30 °C, or 40 °C in protiated solvent (20 mM Tris, 100 mM NaCl; 500 μM DMPC, pH 8.0). Development of bimodal isotope envelopes reflects progressive LPL unfolding. (B) Turbidity reflecting protein aggregation was used as proxy for the melting temperatures (T_m) of LPL^{S132A/R297A} in the presence of APOC2^{WT}, APOC2^{Q70E}, or GPIHBP1. APOC2^{WT} and GPIHBP1 increase thermostability of LPL^{S132A/R297A} by >20 °C (compared to APOC2^{Q70E}), corroborating findings with pulse labeling HDX-MS (A).

protected LPL from temperature-induced unfolding as efficiently as GPIHBP1 (Fig. 5A).

In earlier studies on bovine LPL stability with differential scanning fluorimetry (nano-DSF), the apparent melting temperature (T_m) of LPL's α/β -hydrolase domain was associated with the onset of protein aggregation (21). We therefore used protein aggregation as a proxy for T_m because the protein mixtures complicated the interpretation of changes in tryptophan fluorescence. As shown in Fig. 5B, the onset of LPL aggregation increased by >20 °C (to 55 °C) in the presence of APOC2^{WT} or GPIHBP1 (in contrast to APOC2^{Q70E}), corroborating our HDX-MS data (Fig. 5A) showing that APOC2 and GPIHBP1 protect against thermal unfolding of LPL to a similar degree.

The Impact of ANGPTL4 on LPL in the Presence of APOC2. Given that GPIHBP1 binding stabilizes LPL and mitigates ANGPTL4-catalyzed LPL unfolding (21, 23), we tested whether APOC2 protects LPL against ANGPTL4-mediated inactivation. We performed a continuous labeling experiment in which 6.7 μM LPL^{S132A/R297A} was preincubated with 10 μM APOC2^{WT} or APOC2^{Q70E} in 500 μM DMPC for 2 min at 25 °C. We then added 10 μM ANGPTL4 to the mixture and immediately diluted it into deuterated solvent at 25 °C. Samples were withdrawn after 5, 15, 25, 100, or 1,000 s, and deuterium uptake was assessed by HDX-MS. We identified 48 peptic LPL peptides, yielding an overall sequence coverage of 78.6%. Deuterium uptake into LPL was complex (reflecting conformational states of LPL induced by the opposing effects of APOC2 and ANGPTL4), but it was clear that APOC2^{WT} protected LPL from ANGPTL4-mediated unfolding (Fig. 6A). In pulse-labeling experiments performed at different temperatures (10 to 40 °C), LPL was unfolded after 4 min at 20 °C in the presence of APOC2^{Q70E} and ANGPTL4. Replacing APOC2^{Q70E} with APOC2^{WT} rescued 15% of the LPL from ANGPTL4-induced unfolding, whereas adding GPIHBP1 preserved 63% of the LPL in its native conformation (SI Appendix, Fig. S13). In aggregate, these studies show that APOC2 protects LPL from ANGPTL4-mediated unfolding, but this protection is not as strong and long-lasting as that provided by GPIHBP1.

In continuous labeling at 25 °C, we observed rapid ANGPTL4-mediated LPL unfolding in several peptides (residues 87 to 99, 131 to 163, and 178 to 184) in the presence of APOC2^{Q70E} (Fig. 6B

and SI Appendix, Figs. S14 and S15). The ANGPTL4-mediated unfolding of LPL's catalytic site proceeded through an intermediate conformation of LPL that was not observed in the presence of APOC2^{WT} (SI Appendix, Fig. S15). It is thus possible that APOC2 binding mitigates ANGPTL4-catalyzed LPL unfolding by preventing the formation of that intermediate LPL conformation.

To pursue the mechanism by which APOC2^{WT} counteracts ANGPTL4-mediated LPL inactivation, we performed a pulse-labeling experiment with a 6.7 μM LPL•APOC2^{WT} complex in the presence of 10 μM ANGPTL4 and 500 μM DMPC (SI Appendix, Fig. S15). Pulse labeling provides structural snapshots that reveal the coexistence of folded and unfolded states in a specific region of a protein (e.g., the active site LPL peptide 131 to 163). The degree of unfolding can be quantified by binomial fitting of the bi- or trimodal isotope envelopes. A time-dependent progression in the intensity of the high-mass fraction signifies that the unfolding is irreversible. Of note, pulse labeling of LPL in the presence of ANGPTL4 and APOC2 produced EX1 exchange kinetics in LPL's active site peptide (131 to 163) that were correlated with results from continuous labeling (Fig. 6C). Correlation was observed in incubations with either APOC2^{WT} or APOC2^{Q70E}, but progression to irreversible unfolding, as judged by deuterium uptake with EX1 exchange kinetics, was retarded only by APOC2^{WT} (Fig. 6D).

In earlier studies, we showed preservation of LPL activity by GPIHBP1 in the presence of ANGPTL4 and suggested that the protection resulted from an allosteric effect of GPIHBP1 (23, 38). In those studies, no correlation was observed between deuterium uptake in the high-mass fraction (EX1) by pulse and continuous labeling at 25 °C, indicating that GPIHBP1 binding allows reversible unfolding of LPL's active site but mitigates subsequent irreversible unfolding (21). These findings are consistent with the fact that GPIHBP1 and ANGPTL4 have independent binding sites on LPL, allowing both proteins to bind simultaneously (21). In contrast, the strong correlation between EX1-mediated deuterium uptake in LPL with pulse and continuous deuterium labeling in the presence of ANGPTL4 and APOC2^{WT} indicates that the mechanism by which APOC2 inhibits ANGPTL4-mediated unfolding is distinct from that of GPIHBP1 (Fig. 6D). In the presence of ANGPTL4, APOC2 competes for binding to LPL, consistent with overlapping binding sites (Figs. 3 and 7). However, whenever APOC2 spontaneously dissociates from LPL, ANGPTL4 is free

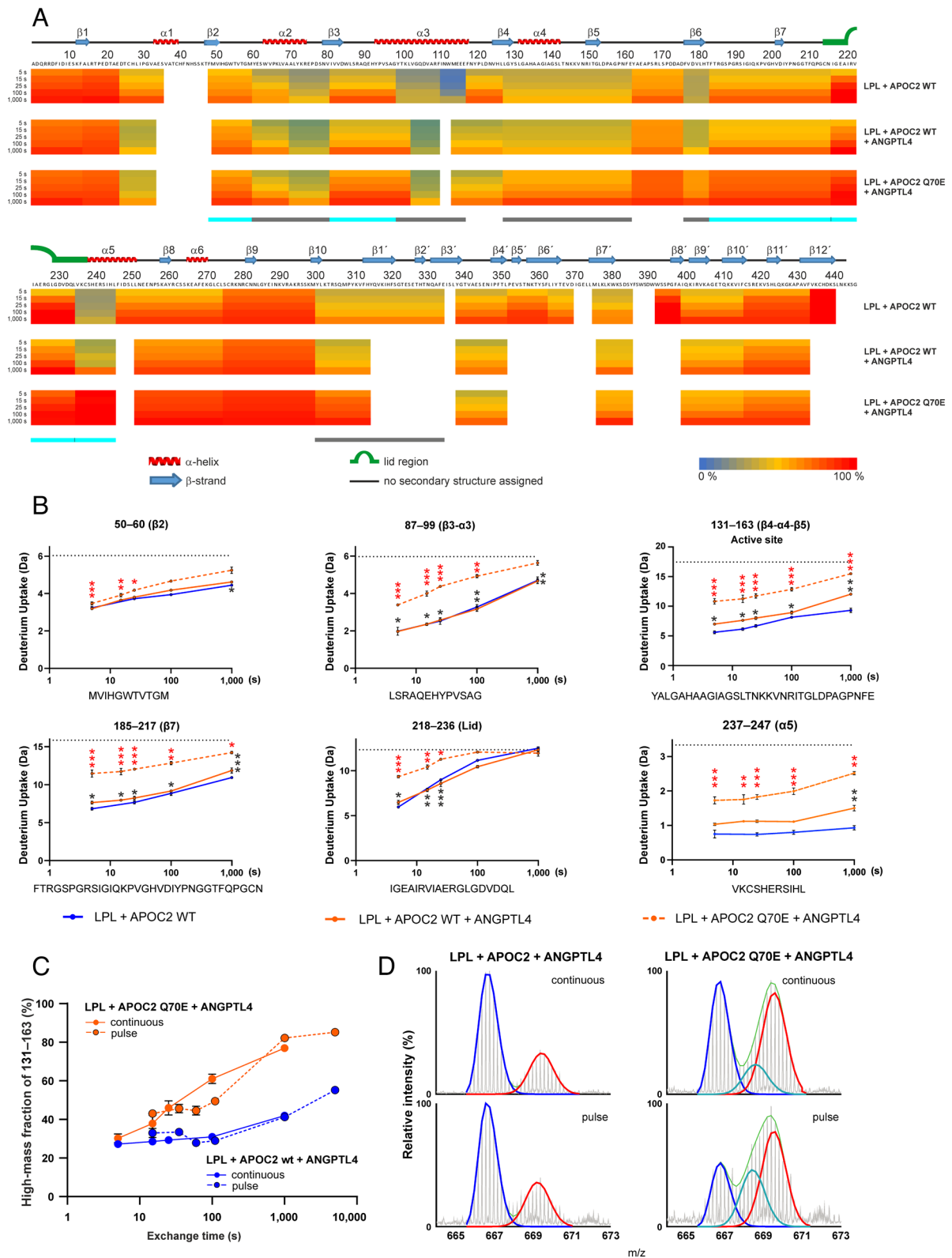


Fig. 6. Interplay between APOC2 and ANGPTL4 in the unfolding of LPL. (A) Heat maps showing the time-dependent deuterium uptake in LPL during continuous deuterium labeling of 3 μM LPL^{S132A/R297A}, 4.5 μM APOC2^{WT}, or APOC2^{Q70E}, and 4.5 μM ANGPTL4 in the presence of 225 μM DMPC at 25 °C. For comparison, we have included data from Fig. 2 on the deuterium uptake in APOC2^{WT}-LPL complexes (i.e., for 3 μM LPL^{S132A/R297A} in the presence of 4.5 μM APOC2^{WT}). (B) Time-dependent deuterium uptake in selected peptic peptides from LPL^{S132A/R297A} incubated in deuterium oxide with APOC2^{WT} (blue), APOC2^{WT} and ANGPTL4 (solid orange), or APOC2^{Q70E} and ANGPTL4 (broken orange). The relative abundance of bimodal isotope envelopes with EX1 kinetics, as judged by visual inspection, are marked with asterisks. Deuterium uptake plots for all peptides are shown in *SI Appendix, Fig. S14*. (C) Relative abundance of high-mass peptide envelopes from EX1 exchange in LPL 131 to 163 (active site in LPL) induced by ANGPTL4 in the presence of APOC2^{WT} (blue) or APOC2^{Q70E} (red). Comparison of pulse and continuous labeling yields similar unfolding kinetics for 131 to 163. (D) Isotope envelopes for 131 to 163 after a 25-s incubation in deuterium oxide (continuous labeling) or after a 25-s incubation in protonated solvent followed by a 10-s pulse in deuterium oxide (pulse labeling). The isotope envelopes were decomposed into three unimodal patterns by binomial fitting using HX-Express2; the low-mass envelope representing the parent folded peptide (blue line), an intermediate state (green line) and the unfolded state (red line). Isotope envelopes for 131 to 163 after continuous and pulse labeling are shown in *SI Appendix, Fig. S15*.

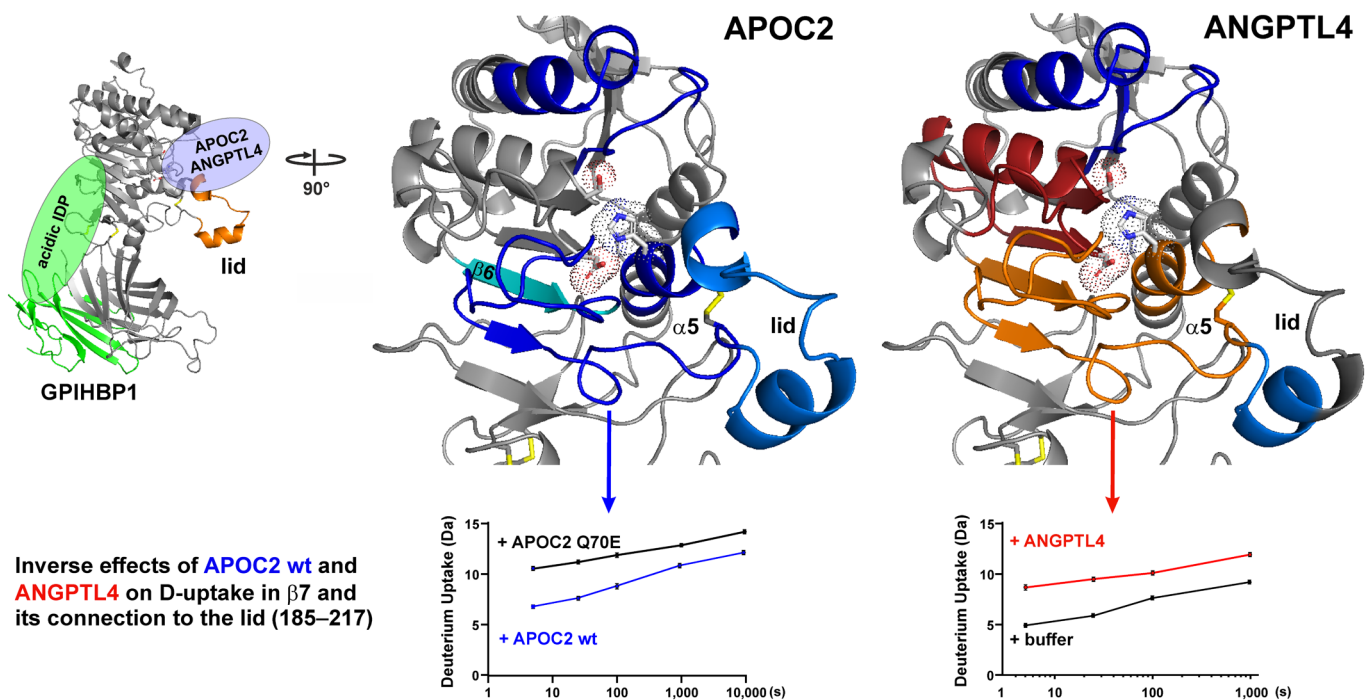


Fig. 7. Differential impact of APOC2 and ANGPTL4 on structural elements forming the catalytic pocket of LPL. The crystal structure of LPL·GPIHBP1 (17) is shown on the *Left* as a ribbon diagram (LPL, gray; GPIHBP1 green). GPIHBP1's intrinsically disordered acidic domain is represented by the green oval, and a modelled structure of LPL's lid is shown in orange. The two structures shown to the *Right* are close-ups of LPL's α/β -hydrolase domain with imprints from APOC2 or ANGPTL4 binding being color-coded; structures with reduced deuterium uptake are shown in blue, while elements with increased deuterium uptake are shown in orange (increased dynamics) and red (subsequent global unfolding). β 6 is colored cyan in the middle figure. Note, ANGPTL4 destabilizes most of the lower half of LPL's catalytic domain (21). The lower panels, show time-dependent deuterium uptake into a lid-anchoring peptide in LPL (β 7 with connecting peptide). The presence of APOC2^{wt} retards deuterium uptake (i.e., reduces mobility), while ANGPTL4 promotes deuterium uptake (i.e., increases mobility) (21). Note, the absolute deuterium uptake cannot be compared between these studies, since the ANGPTL4 experiments needed to be performed with LPL complexed to GPIHBP1 to gain sufficient LPL stability to complete the time course experiment (24).

to engage the vacant binding site on LPL and catalyze LPL unfolding.

Discussion

In earlier studies, we used HDX-MS and X-ray crystallography to define binding interfaces between LPL and GPIHBP1 (17, 20), ANGPTL4 (21), and the LPL-specific monoclonal antibody 5D2 (19, 51). With HDX-MS, we discovered that ANGPTL4 inhibits LPL by binding to the α/β -hydrolase domain and triggering conformational changes that result in the collapse of LPL's catalytic pocket and irreversible enzyme inactivation (14, 19, 21). The ANGPTL4-catalyzed unfolding of LPL was counteracted by GPIHBP1 (23). In the current studies, we used HDX-MS to define interactions between APOC2 and LPL. First, we defined the binding interface between APOC2 and LPL's α/β -hydrolase domain, and found, to our surprise, that the interface overlaps with the binding site for ANGPTL4. Second, we observed that APOC2 binding stabilizes LPL, thereby delaying spontaneous LPL unfolding. Third, we showed that APOC2-bound LPL is less susceptible to ANGPTL4-mediated unfolding due to the fact that they compete for the same site on LPL. Additional studies suggested that the stabilizing effects of APOC2 binding and the destabilizing effects of ANGPTL4 binding on LPL are a consequence of distinct effects on the conformational dynamics of sequences that anchor the lid to the α/β -hydrolase domain.

An interaction between LPL and APOC2 helix III had been previously observed (44, 52) and was further documented by the current studies; however, the identity of the binding site(s) on LPL was not clear and remained controversial. Early studies with an LPL–hepatic lipase chimera suggested that the C-terminal 60

amino acids of LPL (residues 389 to 448) were important for APOC2 activity (47). Subsequently, photoaffinity crosslinking studies with a synthetic C-terminal APOC2 fragment (residues 44 to 79) were used in an attempt to map APOC2's binding site on LPL (45). In those studies, the APOC2 fragment was crosslinked to LPL residues 65 to 86 (α 2– β 3), which was interpreted to be the APOC2 binding site. However, these crosslinking studies have limitations. Because crosslinkers and spacers are bulky, they often cannot be accommodated within binding interfaces; consequently, they rarely react with sequences within the interface and instead react with residues at a distance from the interface (53, 54). In the current study, we used HDX-MS to map the binding site for APOC2 on LPL; this method reports on the solvent exposure of backbone amides of proteins, which is perturbed when proteins are engaged in a complex. We discovered that APOC2 reduced deuterium uptake in four distinct regions in LPL (residues 50 to 60, 87 to 99, 185 to 217, and 218 to 236)—all surrounding the catalytic pocket in LPL's α/β -hydrolase domain and none within LPL's C-terminal domain (Fig. 7). None of these regions coincide with the photoaffinity crosslinking site (residues 65 to 86) (45). As one might have predicted, residues 65 to 86 are at the periphery of the APOC2–LPL binding interface (*SI Appendix, Fig. S8B*). The APOC2 binding site, as defined by HDX-MS, contains key parts of LPL's catalytic machinery, including the oxyanion hole (Trp⁵⁵), part of the catalytic triad (His²⁴¹), and the lid region (residues 217 to 238). By interacting with these structures, APOC2 is positioned to control the movement of the lid and thereby regulate the entry of lipid substrates to the active site (conformational gating).

A comparison of the binding sites on LPL for APOC2 (in the current study) and the binding site of ANGPTL4 (21) revealed

both similarities and differences (Fig. 7). Despite having opposite impacts on LPL activity, APOC2 and ANGPTL4 both engage three regions surrounding LPL's catalytic pocket, evident by reduced deuterium uptake in LPL peptic peptides spanning residues 50 to 60 (connecting β 2 and α 2), 87 to 99 (connecting β 3 and α 3), and 218 to 236 (lid). The fact that APOC2 bound to the lid is not surprising, given APOC2's ability to activate LPL and promote triglyceride hydrolysis. Earlier studies examined hybrid LPL proteins containing lids from structurally related lipases that are not activated by APOC2, for example, hepatic lipase (55) and endothelial lipase (56). APOC2 activated an LPL hybrid containing an EL lid, but failed to activate an EL hybrid with an LPL lid (56). At face value, those findings suggest that APOC2 interactions with the lid are not exclusively responsible for LPL activation. The fact that the APOC2 binding site involves not only the lid (residues 218 to 236) but also loops connecting β 2 to α 2 (residues 50 to 60), β 3 to α 3 (87 to 99), β 7 to the lid (185 to 217) (Fig. 7 and *SI Appendix, Fig. S8B*) implies a more complex mechanism for APOC2 activity—and one that cannot be fully understood with lid-swapping experiments.

Our time-resolved HDX-MS datasets for LPL bound to APOC2 or ANGPTL4 (21) allowed us to glean insights into the allosteric regulation of LPL. A comparison of these data sets revealed that APOC2 and ANGPTL4 have inverse effects on the conformational dynamics in regions of LPL that connect the lid to the α/β -hydrolase domain. The N-terminal anchoring site of LPL's lid is β 7 and connecting loops (residues 185 to 217). APOC2 binding to LPL reduces deuterium uptake in that region (Fig. 3C), whereas ANGPTL4 binding increases deuterium uptake (21). Both effects occur promptly (observed after 5 s), are long-lasting, and are governed by EX2 exchange kinetics (Fig. 7). These findings imply that APOC2 uses this region as a part of its binding interface with LPL, whereas ANGPTL4 uses the same region to trigger allosteric changes that destabilize the α/β -hydrolase domain and lead to enzyme inactivation. The C-terminal end of LPL's lid sequence is anchored to α 5 (237 to 247). The inverse effects of APOC2 and ANGPTL4 on deuterium uptake were also evident in that region but with different kinetics. The destabilizing effect of ANGPTL4 occurs promptly (21), whereas the stabilizing effect of APOC2 was evident only at later time points (when LPL unfolding was evident in the presence of APOC2^{Q70E}) (Fig. 3C).

Our studies provide new insights into the molecular regulation of LPL by APOC2 and ANGPTL4. We find that APOC2 and ANGPTL4 differentially affect the conformational dynamics of structural elements that anchor the lid, providing a plausible explanation for their opposing effects on LPL activity. We propose that the stabilizing effects of APOC2 on LPL's lid-anchoring sequences are crucial for the positioning of the lid and for conformational gating of LPL's active site. Although this proposition needs further testing, a link between the dynamics of LPL's lid-anchoring structures and conformational gating is quite plausible. In the case of monoacylglycerol lipase, mutating the catalytic triad aspartate (Asp²³⁹) caused the lid to assume a closed and inactive conformation (57), and that structural change was accompanied by increased dynamics in the sequences that anchored the lid to the α/β -hydrolase domain. In light of those observations, it is easy to imagine that the stabilizing effects of APOC2 on lid-anchoring sequences are accompanied by an open lid conformation and conformational gating of LPL activity.

The activation of pancreatic lipase by its cofactor (colipase) involves direct interactions between colipase and the lid domain. A crystal structure of the colipase–pancreatic lipase complex revealed a well-defined binding interface between the lid and

colipase loops (58). In our studies, we found, by HDX-MS, that APOC2 interacts both with LPL's lid and lid-anchoring sequences. Whether APOC2 binding promotes an open conformation of LPL's lid (and conformational gating) indirectly by stabilizing the lid-anchoring regions or simply by direct interaction with the lid (as was the case with pancreatic lipase) remains to be clarified. Solving the structure of the LPL•APOC2 complex by X-ray crystallography or cryo-EM would help to clarify this issue. In future studies, it will be important to define the binding interface (and downstream allosteric effects) of short APOC2 mimetic peptides. APOC2 mimetic peptides have been shown to activate LPL and reduce plasma triglyceride levels in mouse models of hypertriglyceridemia and could prove to be useful for treating the hypertriglyceridemia in patients with APOC2 deficiency (41).

Materials and Methods

Purified Proteins and Chemicals. Human LPL (residues 1 to 448) as well as an inactive LPL mutant with a substitution in a catalytic triad residue (S132A) and a substitution that eliminates a furin cleavage site (R297A) were produced in *Drosophila* S2 cells and purified by heparin–Sepharose affinity chromatography (22). A soluble truncated version of human GPIIIBP1 (residues 1 to 131) was produced in *Drosophila* S2 cells and purified as described (20). The coiled-coil domain of human ANGPTL4 (residues 1 to 159 with an N-terminal methionine and a C-terminal 6×His tag) was produced in *Escherichia coli* BL21 (DE3) with a pet29a vector (59). DMPC was from Avanti Lipids, free fatty acid-free bovine serum albumin and Intralipid™ were from Sigma-Aldrich, and NEFA-HR 2 kit was from Wako Chemicals.

Preparation of APOC2. APOC2 with an N-terminal 6×His-tag was expressed in *E. coli* BL21(DE3) (44). After induction, the cell pellet was dissolved in 20 mM Tris, 100 mM NaCl, 2 M urea, 2% (v/v) Triton X-100, 1 mM PMSF, pH 8.0, and stored at -20°C . Cells were disrupted by sonication (10 cycles of 30 s) at 4°C ; the suspension was centrifuged at 4°C for 30 min at $30,000 \times g$; and the supernatant was passed through a 0.2- μm filter and applied to 1-mL His column at a flow rate of 0.5 mL/min. After extensive washing, first with 20 mM Tris-HCl, 100 mM NaCl, 2 M urea, and 0.05% (v/v) Triton X-100 (pH 8.0) and then with the same buffer supplemented with 50 mM imidazole, proteins were eluted with 250 mM imidazole in the same buffer. The elution profile was evaluated by Coomassie blue staining after sodium dodecyl sulfate polyacrylamide gel electrophoresis (SDS-PAGE). Peak fractions were subjected to Superdex G75 size-exclusion chromatography. Peak fractions were pooled and dialyzed against 20 mM Tris, 100 mM NaCl, and 0.05% Triton X-100 (pH 8.0) and stored as aliquots at -20°C . For HDX-MS experiments, Triton X-100 was removed from APOC2 using Pierce™ Detergent Removal Spin Column (Thermo Scientific™).

Additional information on HDX-MS, nano-DSF, CD, and are LPL activity assays are listed in (*SI Appendix, Materials & Methods*).

Data, Materials, and Software Availability. All study data are included in the article and/or *SI Appendix*.

ACKNOWLEDGMENTS. We thank Gry Ellis Rasmussen and Eva C. Østerlund for technical assistance. Supported by grants from the NOVO Nordisk Foundation Grants (NNF18OC0033864 and NNF20OC0063444); the European Union's Horizon 2020 research and innovation program under the Marie Skłodowska-Curie grant agreement No 801481; The John and Birthe Meyer Foundation; and the National Heart, Lung, and Blood Institute (HL146358, HL087228, and HL139725).

Author affiliations: ^aFinsen Laboratory, Copenhagen University Hospital-Rigshospitalet, DK-2200 Copenhagen N, Denmark; ^bFinsen Laboratory, Biotech Research and Innovation Centre, University of Copenhagen, DK-2200 Copenhagen N, Denmark; ^cDepartment of Biochemistry and Molecular Biology, University of Southern Denmark, DK-5320 Odense, Denmark; ^dDepartment of Medicine, David Geffen School of Medicine, University of California, Los Angeles, CA 90095; and ^eDepartment of Human Genetics, David Geffen School of Medicine, University of California, Los Angeles, CA 90095

1. A. V. Khera *et al.*, Association of rare and common variation in the lipoprotein lipase gene with coronary artery disease. *JAMA* **317**, 937–946 (2017).
2. R. Do *et al.*, Common variants associated with plasma triglycerides and risk for coronary artery disease. *Nat. Genet.* **45**, 1345–1352 (2013).
3. L. A. Lotta *et al.*, Association of genetically enhanced lipoprotein lipase-mediated lipolysis and low-density lipoprotein cholesterol-lowering alleles with risk of coronary disease and type 2 diabetes. *JAMA Cardiol.* **3**, 957–966 (2018).
4. D. G. Thomas, Y. Wei, A. R. Tall, Lipid and metabolic syndrome traits in coronary artery disease: A Mendelian randomization study. *J. Lipid Res.* **62**, 100044 (2021).
5. A. R. Tall, D. G. Thomas, A. G. Gonzalez-Cabodevilla, I. J. Goldberg, Addressing dyslipidemic risk beyond LDL-cholesterol. *J. Clin. Invest.* **132**, e148559 (2022).
6. J. S. Dron, R. A. Hegele, Genetics of hypertriglyceridemia. *Front. Endocrinol. (Lausanne)* **11**, 455 (2020).
7. A. B. Jorgensen, R. Frikke-Schmidt, B. G. Nordestgaard, A. Tybjaerg-Hansen, Loss-of-function mutations in APOC3 and risk of ischemic vascular disease. *N. Engl. J. Med.* **371**, 32–41 (2014).
8. F. E. Dewey *et al.*, Inactivating variants in ANGPTL4 and risk of coronary artery disease. *N. Engl. J. Med.* **374**, 1123–1133 (2016).
9. N. O. Stitzel *et al.*, ANGPTL3 deficiency and protection against coronary artery disease. *J. Am. Coll. Cardiol.* **69**, 2054–2063 (2017).
10. P. Helkkula *et al.*, ANGPTL8 protein-truncating variant associated with lower serum triglycerides and risk of coronary disease. *PLoS Genet.* **17**, e1009501 (2021).
11. J. Visser, W. van Zwo, J. A. Kuivenhoven, Managing of dyslipidaemia characterized by accumulation of triglyceride-rich lipoproteins. *Curr. Atheroscler. Rep.* **24**, 1–12 (2022).
12. E. D. Korn, Clearing factor, a heparin-activated lipoprotein lipase. I. Isolation and characterization of the enzyme from normal rat heart. *J. Biol. Chem.* **215**, 1–14 (1955).
13. W. V. Brown, R. I. Levy, D. S. Fredrickson, Further characterization of apolipoproteins from the human plasma very low density lipoproteins. *J. Biol. Chem.* **245**, 6588–6594 (1970).
14. K. K. Kristensen *et al.*, GPIHBP1 and ANGPTL4 utilize protein disorder to orchestrate order in plasma triglyceride metabolism and regulate compartmentalization of LPL activity. *Front. Cell Dev. Biol.* **9**, 702508 (2021).
15. S. G. Young *et al.*, GPIHBP1 and lipoprotein lipase, partners in plasma triglyceride metabolism. *Cell Metab.* **30**, 51–65 (2019).
16. K. L. Sylvers-Davie, B. S. J. Davies, Regulation of lipoprotein metabolism by ANGPTL3, ANGPTL4, and ANGPTL8. *Am. J. Physiol. Endocrinol. Metab.* **321**, E493–E508 (2021).
17. G. Birrane *et al.*, Structure of the lipoprotein lipase-GPIHBP1 complex that mediates plasma triglyceride hydrolysis. *Proc. Natl. Acad. Sci. U.S.A.* **116**, 1723–1732 (2019).
18. A. P. Beigneux *et al.*, Lipoprotein lipase is active as a monomer. *Proc. Natl. Acad. Sci. U.S.A.* **116**, 6319–6328 (2019).
19. K. K. Kristensen *et al.*, Unfolding of monomeric lipoprotein lipase by ANGPTL4: Insight into the regulation of plasma triglyceride metabolism. *Proc. Natl. Acad. Sci. U.S.A.* **117**, 4337–4346 (2020).
20. S. Mysling *et al.*, The acidic domain of the endothelial membrane protein GPIHBP1 stabilizes lipoprotein lipase activity by preventing unfolding of its catalytic domain. *Elife* **5**, e12095 (2016).
21. K. Z. Leth-Espensen *et al.*, The intrinsic instability of the hydrolase domain of lipoprotein lipase facilitates its inactivation by ANGPTL4-catalyzed unfolding. *Proc. Natl. Acad. Sci. U.S.A.* **118**, e2026650118 (2021).
22. A. M. Lund Winther, K. K. Kristensen, A. Kumari, M. Ploug, Expression and one-step purification of active LPL contemplated by biophysical considerations. *J. Lipid Res.* **62**, 100149 (2021).
23. S. Mysling *et al.*, The angiopoietin-like protein ANGPTL4 catalyzes unfolding of the hydrolase domain in lipoprotein lipase and the endothelial membrane protein GPIHBP1 counteracts this unfolding. *Elife* **5**, e20958 (2016).
24. A. M. Lund Winther, A. Kumari, S. G. Young, M. Ploug, ANGPTL4 sensitizes lipoprotein lipase to PCSK3 cleavage by catalyzing its unfolding. *J. Lipid Res.* **62**, 100071 (2021).
25. V. Sukonina, A. Lookene, T. Olivecrona, G. Olivecrona, Angiopoietin-like protein 4 converts lipoprotein lipase to inactive monomers and modulates lipase activity in adipose tissue. *Proc. Natl. Acad. Sci. U.S.A.* **103**, 17450–17455 (2006).
26. Y. Q. Chen *et al.*, Angiopoietin-like protein 8 differentially regulates ANGPTL3 and ANGPTL4 during postprandial partitioning of fatty acids. *J. Lipid Res.* **61**, 1203–1220 (2020).
27. F. Oldoni *et al.*, ANGPTL8 has both endocrine and autocrine effects on substrate utilization. *JCI Insight* **5**, e138777 (2020).
28. O. Kovrov, K. K. Kristensen, E. Larsson, M. Ploug, G. Olivecrona, On the mechanism of angiopoietin-like protein 8 for control of lipoprotein lipase activity. *J. Lipid Res.* **60**, 783–793 (2019).
29. W. Song *et al.*, Electrostatic sheathing of lipoprotein lipase is essential for its movement across capillary endothelial cells. *J. Clin. Invest.* **132**, e157500 (2022).
30. B. S. Davies *et al.*, GPIHBP1 is responsible for the entry of lipoprotein lipase into capillaries. *Cell Metab.* **12**, 42–52 (2010).
31. C. N. Goulbourne *et al.*, The GPIHBP1-LPL complex is responsible for the margination of triglyceride-rich lipoproteins in capillaries. *Cell Metab.* **19**, 849–860 (2014).
32. J. G. Lima *et al.*, A novel GPIHBP1 mutation related to familial chylomicronemia syndrome: A series of cases. *Atherosclerosis* **322**, 31–38 (2021).
33. W. Plengpanich *et al.*, Multimerization of glycosylphosphatidylinositol-anchored high density lipoprotein-binding protein 1 (GPIHBP1) and familial chylomicronemia from a serine-to-cysteine substitution in GPIHBP1 Ly6 domain. *J. Biol. Chem.* **289**, 19491–19499 (2014).
34. G. Olivecrona *et al.*, Mutation of conserved cysteines in the Ly6 domain of GPIHBP1 in familial chylomicronemia. *J. Lipid Res.* **51**, 1535–1545 (2010).
35. A. P. Beigneux *et al.*, Autoantibodies against GPIHBP1 as a cause of hypertriglyceridemia. *N. Engl. J. Med.* **376**, 1647–1658 (2017).
36. K. Miyashita *et al.*, Chylomicronemia from GPIHBP1 autoantibodies. *J. Lipid Res.* **61**, 1365–1376 (2020).
37. J. M. Leth *et al.*, Evolution and medical significance of LU domain-containing proteins. *Int. J. Mol. Sci.* **20**, 2760 (2019).
38. K. K. Kristensen *et al.*, A disordered acidic domain in GPIHBP1 harboring a sulfated tyrosine regulates lipoprotein lipase. *Proc. Natl. Acad. Sci. U.S.A.* **115**, E6020–E6029 (2018).
39. W. K. Sonnenburg *et al.*, GPIHBP1 stabilizes lipoprotein lipase and prevents its inhibition by angiopoietin-like 3 and angiopoietin-like 4. *J. Lipid Res.* **50**, 2421–2429 (2009).
40. A. Wolska *et al.*, Apolipoprotein C-II: New findings related to genetics, biochemistry, and role in triglyceride metabolism. *Atherosclerosis* **267**, 49–60 (2017).
41. A. Wolska *et al.*, A dual apolipoprotein C-II mimetic-apolipoprotein C-III antagonist peptide lowers plasma triglycerides. *Sci. Transl. Med.* **12**, eaaw7905 (2020).
42. J. Zdunek *et al.*, Global structure and dynamics of human apolipoprotein CII in complex with micelles: Evidence for increased mobility of the helix involved in the activation of lipoprotein lipase. *Biochemistry* **42**, 1872–1889 (2003).
43. C. A. MacRaid, G. J. Howlett, P. R. Gooley, The structure and interactions of human apolipoprotein C-II in dodecyl phosphocholine. *Biochemistry* **43**, 8084–8093 (2004).
44. Y. Shen, A. Lookene, S. Nilsson, G. Olivecrona, Functional analyses of human apolipoprotein CII by site-directed mutagenesis: Identification of residues important for activation of lipoprotein lipase. *J. Biol. Chem.* **277**, 4334–4342 (2002).
45. T. L. McIlhargey, Y. Yang, H. Wong, J. S. Hill, Identification of a lipoprotein lipase cofactor-binding site by chemical cross-linking and transfer of apolipoprotein C-II-responsive lipolysis from lipoprotein lipase to hepatic lipase. *J. Biol. Chem.* **278**, 23027–23035 (2003).
46. R. C. Davis *et al.*, Chimeras of hepatic lipase and lipoprotein lipase. Domain localization of enzyme-specific properties. *J. Biol. Chem.* **267**, 21499–21504 (1992).
47. J. S. Hill *et al.*, Subdomain chimeras of hepatic lipase and lipoprotein lipase. Localization of heparin and cofactor binding. *J. Biol. Chem.* **273**, 30979–30984 (1998).
48. T. M. Ryan *et al.*, Apolipoprotein C-II adopts distinct structures in complex with micellar and submicellar forms of the amyloid-inhibiting lipid-mimetic dodecylphosphocholine. *Biophys. J.* **110**, 85–94 (2016).
49. Y. Mao *et al.*, Hydrogen/Deuterium exchange and molecular dynamics analysis of amyloid fibrils formed by a D69K charge-pair mutant of human apolipoprotein C-II. *Biochemistry* **54**, 4805–4814 (2015).
50. K. K. Kristensen, K. Z. Leth-Espensen, S. G. Young, M. Ploug, ANGPTL4 inactivates lipoprotein lipase by catalyzing the irreversible unfolding of LPL's hydrolase domain. *J. Lipid Res.* **61**, 1253 (2020).
51. J. G. Luz *et al.*, The structural basis for monoclonal antibody 5D2 binding to the tryptophan-rich loop of lipoprotein lipase. *J. Lipid Res.* **61**, 1347–1359 (2020).
52. Y. Shen, A. Lookene, L. Zhang, G. Olivecrona, Site-directed mutagenesis of apolipoprotein CII to probe the role of its secondary structure for activation of lipoprotein lipase. *J. Biol. Chem.* **285**, 7484–7492 (2010).
53. L. Piersimoni, P. L. Kastiris, C. Arlt, A. Sinz, Cross-linking mass spectrometry for investigating protein conformations and protein-protein interactions. A method for all seasons. *Chem. Rev.* **122**, 7500–7531 (2022).
54. H. Gardsvoll *et al.*, Characterization of the functional epitope on the urokinase receptor. Complete alanine scanning mutagenesis supplemented by chemical cross-linking. *J. Biol. Chem.* **281**, 19260–19272 (2006).
55. K. A. Dugi, H. L. Dichek, G. D. Talley, H. B. Brewer Jr., S. Santamarina-Fojo, Human lipoprotein lipase: The loop covering the catalytic site is essential for interaction with lipid substrates. *J. Biol. Chem.* **267**, 25086–25091 (1992).
56. N. Griffon *et al.*, Substrate specificity of lipoprotein lipase and endothelial lipase: Studies of lid chimeras. *J. Lipid Res.* **47**, 1803–1811 (2006).
57. S. Tyukhtenko *et al.*, Conformational gating, dynamics and allostery in human monoacylglycerol lipase. *Sci. Rep.* **10**, 18531 (2020).
58. H. van Tilbeurgh *et al.*, Interfacial activation of the lipase-prolipase complex by mixed micelles revealed by X-ray crystallography. *Nature* **362**, 814–820 (1993).
59. T. Robal, M. Larsson, M. Martin, G. Olivecrona, A. Lookene, Fatty acids bind tightly to the N-terminal domain of angiopoietin-like protein 4 and modulate its interaction with lipoprotein lipase. *J. Biol. Chem.* **287**, 29739–29752 (2012).